JMEPEG (2012) 21:1380–1390
DOI: 10.1007/s11665-011-0013-2

1059-9495/$19.00

Damage Characterization of Glass/Epoxy Composite Under Three-Point Bending Test Using Acoustic Emission Technique

Farzad Pashmforoush, Mohamad Fotouhi, and Mehdi Ahmadi

(Submitted February 1, 2011; in revised form July 3, 2011)

Acoustic emission (AE) technique is an efficient non-destructive method for detection and identification of various damage mechanisms in composite materials. Discrimination of AE signals related to different damage modes is of great importance in the use of this technique. For this purpose, integration of *k*-means algorithm and genetic algorithm (GA) was used in this study to cluster AE events of glass/epoxy composite during three-point bending test. Performing clustering analysis, three clusters with separate frequency ranges were obtained, each one representing a distinct damage mechanism. Furthermore, time-frequency analysis of AE signals was performed based on wavelet packet transform (WPT). In order to find the dominant components associated with different damage mechanisms, the energy distribution criterion was used. The frequency ranges of the dominant components were then compared with *k*-means genetic algorithm (KGA) outputs. Finally, SEM observation was utilized to validate the results. The obtained results indicate good performance of the proposed methods in the damage characterization of composite materials.

Keywords Acoustic emission, Composite materials, Damage characterization, *k*-means genetic algorithm, Wavelet packet transform

1. Introduction

Fiber-reinforced plastic (FRP) composite materials are extensively used in various engineering applications because of their high specific stiffness and strength. However, various damage mechanisms may degrade the long-term performance of these materials. Delamination is one of the most significant failure modes in composites because of its considerable effect on the reduction of the material residual strength and fatigue life (Ref 1, 2). Hence, its detection is really an important task. Acoustic emission (AE) technique is an efficient non-destructive method for detection and identification of various damage types in composite materials. AE phenomenon is the result of transient elastic wave generated by a rapid release of energy within a material because of changes in local stress and strain fields (Ref 3). AE signals mostly originate from various sources, such as matrix cracking, fiber breakage, delamination, and debonding (Ref 4, 5). Hence, discrimination of AE signals corresponding to different failure mechanisms is of great importance in the use of AE technique. In order to find the relationship between AE parameters and damage mechanisms, several studies have been conducted using different AE features such as counts, amplitude, energy, etc. (Ref 6-8). Also, there are various researches that have used multiparameter analysis to improve discrimination of AE events (Ref 9-11). Kenji and ono (Ref 12) used supervised pattern recognition based on the *k*-nearest algorithm for identification of damage modes in carbon fiber/epoxy composites. Supervised pattern recognition is used whenever the number of damage mechanisms is known before, while unsupervised pattern recognition is performed without any previous knowledge. Moevu et al. (Ref 13) applied unsupervised pattern recognition algorithm on AE signals obtained from two SiCf/[Si-B-C] composites and could successfully distinguish between different types of matrix cracking.

Kohonen's self-organizing map (SOM) is a neural network algorithm used by several researchers for clustering AE signals (Ref 14-16). Godin et al. (Ref 17) used integration of Kohonen's som and *k*-means algorithm for classification of AE events of glass/epoxy composites and obtained interesting results. Neural network approach, although accurate, suffers from a large computational time. Moreover, its performance is dependent on network structure and number of neurons which must be specified previously (Ref 18).

Most of the above mentioned studies have been performed in time domain, while valuable information can be achieved using frequency domain. Ni and Iwamoto (Ref 19) used wavelet transform to study the relationship between AE signals and damage sources and concluded that frequency analysis is an efficient way for processing AE signals of composite materials.

Marec et al. (Ref 20) used continuous and discrete wavelet transform to extract new time-scale descriptors to improve the characterization of damage mechanisms. They applied fuzzy *c*-means clustering associated with a principal component analysis (PCA) to cluster the AE events. The results showed

Farzad Pashmforoush, Mohamad Fotouhi, and **Mehdi Ahmadi**, Non-Destructive Testing Lab, Department of Mechanical Engineering, Amirkabir University of Technology, 424 Hafez Avenue, 15914 Tehran, Iran. Contact e-mails: f.pashmfroush@yahoo.com and ahmadin@aut.ac.ir.

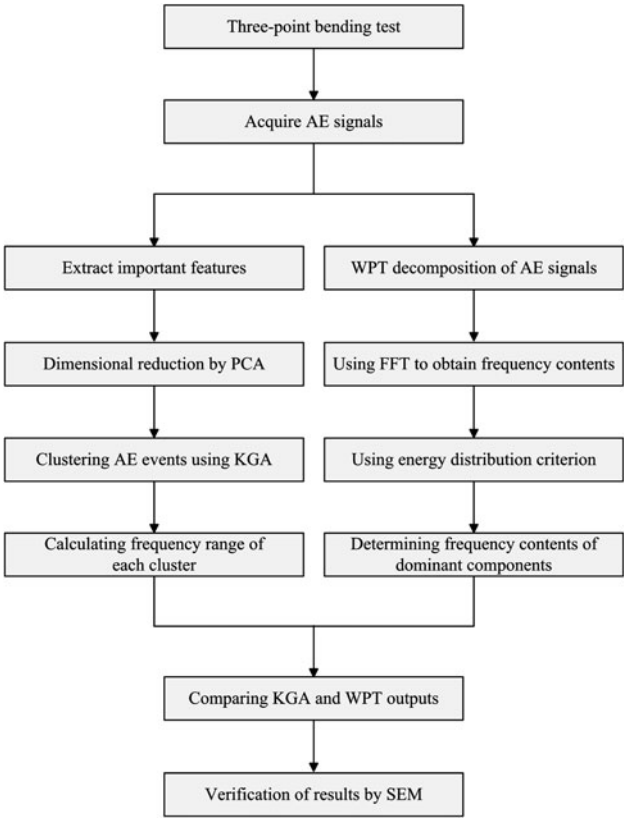

Fig. 1 Brief explanation of damage characterization procedure

that the new descriptors could provide a better discrimination of damage mechanisms.

In this article PCA was first employed to reduce the dimensionality of rather large data without much loss of information. The AE signals used for clustering analysis were collected during the quasi-static three-point bending test with starter delamination crack. After dimensional reduction, the datasets were clustered using integration of genetic algorithm (GA) and *k*-means algorithm. *k*-Means algorithm is one of the most widely used clustering algorithms, however, its performance strongly depends on the initial cluster centers and it may get stuck at local minima. In order to overcome this problem, GA was used as an effective technique to find optimum cluster centers. Indeed, the searching capability of GA can provide an optimal solution in a reasonable time.

Also in this study, time-frequency analysis of AE signals was performed using wavelet packet transform (WPT). AE signals were first decomposed into a set of wavelet components, each having its specific frequency range. Then, energy criterion was used for analyzing each level of AE signals. Applying this criterion, the dominant components related to different damage modes were obtained. Finally, after comparing *k*-means genetic algorithm (KGA) and WPT outputs, the obtained results were verified using microscopic observation by SEM. A brief explanation of damage characterization procedure is shown in Fig. 1.

2. Experimental Procedure

The composite materials used in this study were made up of epoxy resin reinforced by E-glass fiber with volume fraction of 60%. Two types of specimens, cross-ply $[0, 90]_{5s}$ and unidirectional $[0]_{10}$, were prepared for the experimental study. The specimens were in rectangular form with blind holes in the center. Also, starter crack was created by inserting a Teflon film with a thickness of about 20 μm as an initial crack for the delamination test. The blind hole was designed to stimulate delamination in bottom plies, i.e., push-out delamination and the pre-crack was utilized to hasten the initiation of delamination. The laminates were fabricated by manual lay-up with mold compression. The dimensions of all the specimens were 150 mm × 50 mm × 5 mm. For ease of operation, the cross-ply specimen is named S1, and the unidirectional specimen is named S2.

Three-point bending tests were performed in a universal test machine with the load cell capacity of 1000 N at the cross-head speed of 0.2 mm/min.

The acoustic emission software AEWin and a data-acquisition system (PAC) PCI-2 with a maximum sampling rate of 40 MHz were used for recording AE activities. A broadband, resonant-type, single-crystal piezoelectric transducer manufactured by Physical Acoustic Corporation (PAC) with operating range of frequencies between 100 and 750 kHz and resonance frequency of 513.28 kHz was used as the AE sensor. For the purpose of good acoustic coupling between the sensor and the specimens, grease was used for covering the surface of the sensor. In order to determine the threshold value, primary experiments were conducted without any applied load. The threshold value of 40 dB could filter the noise of ambient and the test device very well. Also, calibration of AE signals was performed in accordance with the standard pencil lead breakage test (Hsu-Nielsen method). The attenuation of AE signals was measured by repeating the lead breakage test at different positions between the AE sensors. AE events were detected by sensor and enhanced by a 2/4/6-AST preamplifier. The gain selector of the preamplifier was set to 40 dB. During the test, the AE signals were monitored by two sensors which were placed in a linear configuration located at a distance of 100 mm, as shown in Fig. 2. Two sensors were used ensuring that only the AE signals of damage area were used for clustering analysis.

3. Clustering Analysis

3.1 Principal Component Analysis (PCA)

The PCA is a multivariate analysis tool commonly used for reducing dimensionality of a large dataset to enable a better visualization and analysis of data (Ref 21). Dimensional reduction is performed by transforming data to a new set of uncorrelated variables, i.e., the principal components (PCS). Indeed, PCA projects the data along the directions that describe maximum variance in the dataset. These directions are determined by the eigenvectors of the covariance matrix with the highest eigenvalues. Let x be the $n \times m$ input datasets, where n and m are the number of AE signals and relevant variables (features), respectively. Since the variables are not in the same units, the data must be standardized. Standardization is done by transforming all the data to have zero mean and unit standard deviation. In this case, all variables have same weight. The next step after data standardization is to calculate covariance matrix. Afterward, eigenvectors and corresponding eigenvalues for covariance matrix have to be calculated. If C denotes the covariance matrix, then the eigenvalues λ_i can be obtained by

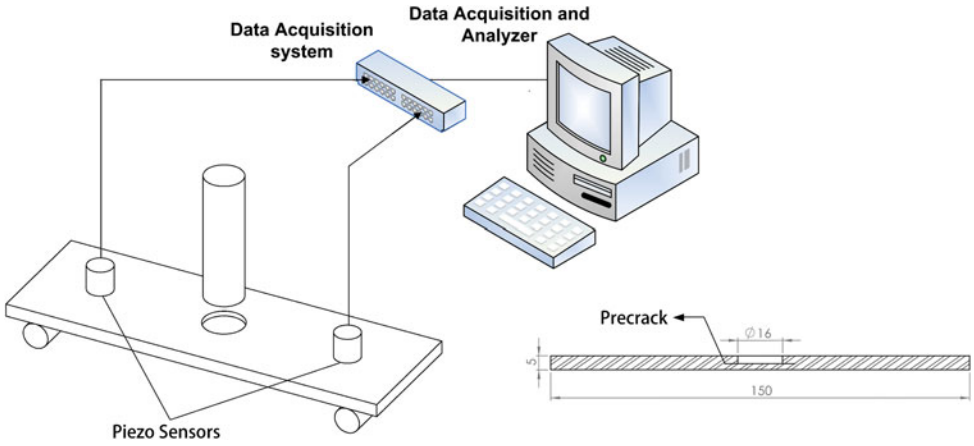

Fig. 2 Shematic of experimental set-up

solving the determinant equation $\det(C - \lambda_i) = 0$. Then, eigenvectors are columns of the matrix A such that $C = ADA^{\mathrm{T}}$, in which

$$D = \begin{bmatrix} \lambda_1 & 0 & \dots & 0 \\ 0 & \lambda_2 & \dots & 0 \\ \vdots & \vdots & \vdots & \vdots \\ 0 & 0 & \dots & \lambda_m \end{bmatrix} \quad \text{(Eq 1)}$$

where $\lambda_1 \geq \lambda_2 \geq \cdots \geq \lambda_m$.

If only first l eigenvectors are kept for clustering analysis, then the transformation to PCS is expressed as

$$y = XA_l \quad \text{(Eq 2)}$$

where A_l $(m \times l)$ denotes the matrix having the first l eigenvectors. It should be mentioned that the cumulative sum of the variances of the first few PCs should be at least 80% of the total variance of the input data.

3.2 k-Means Algorithm

The objective of k-means algorithm is to classify a set of n data points in m-dimensional space into k number of classes (Ref 22). The classification is done by minimizing the sum of squares of distances between data and the respective cluster centers. The first step of k-means algorithm is to partition the input data into k initial sets. After calculating mean point (centroid), a new partition is constructed by assigning each point to the cluster with the nearest center. Then, the new centroids are recalculated for the new clusters, and the algorithm is repeated by alternate application of these two steps until the coordinates of cluster centers do not change any more. Since the number of classes is not known a priori, the algorithm must be executed for different values of k, and the best partitioning must be defined by means of a validity criteria such as the Davis-Bouldin (DB) index (Ref 23). The DB index is calculated as follows:

$$\mathrm{DB} = \frac{1}{k}\sum_{i=1}^{k} \max_{i \neq j}\left\{\frac{s_i + s_j}{d_{ij}}\right\} \quad \text{(Eq 3)}$$

where s is the within-cluster distance, d is the between clusters distance, and k is the number of clusters. The low values of DB index indicate good clustering.

3.3 k-Means Genetic Algorithm

The drawback of k-means algorithm is that its performance strongly depends on the choice of the initial cluster centers, and it often gets stuck at local minima. In order to solve this problem, integration of k-means algorithm and genetic algorithm is proposed as an effective clustering technique (Ref 24, 25). Combining the simplicity of k-means algorithm with the capability of GAs in avoiding local optima can provide an optimum clustering of AE events.

The steps of KGA are as follows:

Step 1 *Chromosome representation*. Each chromosome is a series of real numbers representing the cluster centers.

Step 2 *Population initialization*. k random points are chosen from input dataset to form cluster centers.

Step 3 *Clustering*. In this step, each point x is assigned to the cluster with the nearest center, and then new centers are calculated by Eq 4:

$$z_i^* = \frac{1}{n_i}\sum_{x_j \in C_i} x_j, \quad i = 1, 2, \dots, k \quad \text{(Eq 4)}$$

where z_i^* is the new cluster center and n_i is the number of points belonging to cluster C_i.

Step 4 *Fitness computation*. Fitness value is defined as the summation of the Euclidean distances of the points from their corresponding cluster centers (Eq 5):

$$\text{Fitness value} = \sum_{i=1}^{k}\sum_{x_j \in C_i} ||x_j - z_i|| \quad \text{(Eq 5)}$$

where z_i denotes cluster center, and k is the number of clusters. For optimum clustering, fitness value must be minimized.

Step 5 *Selection*. Two parents are selected from a population according to their fitness to create two new children. In this study, Roulette wheel selection with elitist selection was used. Elitist selection, which copies at least one best solution without any changes to a new population, guarante the best solution ever found to survive till the end.

Step 6 *Crossover*. In this step, two parents exchange their information to create new children with a specified crossover probability.

Table 1 Initial parameters of KGA

Initial population	Crossover rate	Mutation rate	Maximum number of iterations
100	0.7	0.01	500

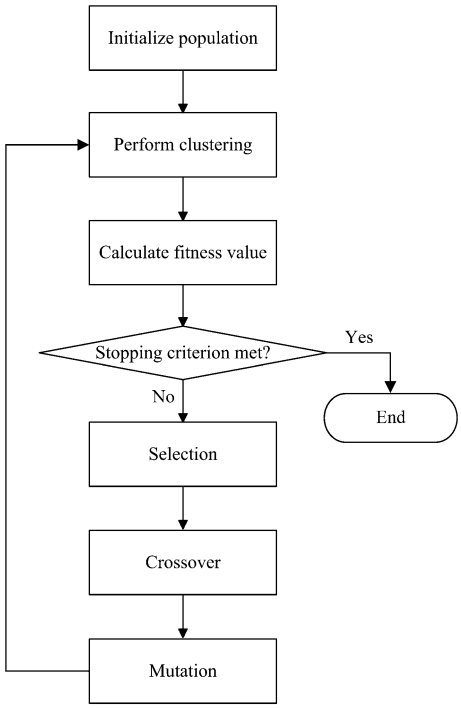

Fig. 3 Flowchart of KGA

Step 7 *Mutation*. After crossover is performed, mutation takes place according to Eq 6:

$$r' = \begin{cases} r \times (1 \pm 2\Delta) & \text{if } r \neq 0 \\ (\pm 2\Delta) & \text{if } r = 0 \end{cases} \quad \text{(Eq 6)}$$

where r and r' are the values are at a gene position before and after mutation, respectively, and Δ is a number in the range [0, 1] generated with uniform distribution. The (+) or (−) sign both have the same probability to occur.

Step 8 *Checking stopping criterion*. The algorithm should be repeated, while the stopping criterion is reached. In this article, the maximum number of iterations was used as stopping criterion.

Table 1 summarizes the initial parameters of KGA. Also, the flowchart of the algorithm is shown in Fig. 3.

3.4 Wavelet Packet Transform

The wavelet transform (WT) is a powerful signal-processing tool introduced in the mid-1980s (Ref 26). WT has been used successfully by various researchers for analyzing AE signals (Ref 27, 28). Wavelet is a waveform of effectively limited duration with zero average value. Let $f(t)$ be an arbitrary square integrable function. Mathematically, the continuous WT of $f(t)$ with respect to a mother wavelet $\psi(t)$ is expressed as

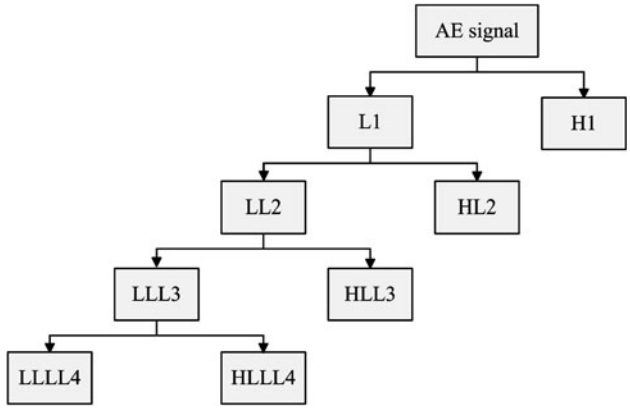

Fig. 4 Discrete wavelet transform decomposition tree

$$\mathrm{CWT}(a,b) = \frac{1}{\sqrt{a}} \int_{-\infty}^{+\infty} f(t)\psi^*\left(\frac{t-b}{a}\right) dt \quad \text{(Eq 7)}$$

where a is the scale parameter, b is the translation parameter, and ψ^* is the complex conjugate of the mother wavelet. The inverse continuous WT is defined by Eq 8 and 9:

$$f(t) = \frac{1}{C} \int_{a=-\infty}^{+\infty} \int_{b=-\infty}^{+\infty} \frac{1}{|a|^2} \mathrm{CWT}(a,b)\, \psi(t)\, da\, db \quad \text{(Eq 8)}$$

$$C = \int_{-\infty}^{+\infty} \frac{|\Psi(\omega)^2|}{\omega} d\omega \quad \text{(Eq 9)}$$

The most common method of discrete WT is to use dyadic scales and translations. In this case, the scale parameter takes values of the form $a = 2^j$, and the translation parameter takes the values of the form $k \cdot 2^j$, where j and k are integers. Mathematically, discrete WT can be described as Eq 10:

$$f(t) = c \sum_j \sum_k \mathrm{DWT}(j,k) 2^{-j/2}\, \psi(2^{-j}t - k) \quad \text{(Eq 10)}$$

Where the wavelet coefficients DWT(j, k) are described by Eq 11:

$$\mathrm{DWT}(j,k) = \int_{-\infty}^{+\infty} f(t) 2^{j/2}\, \psi^*(2^j t - k)\, dt \quad \text{(Eq 11)}$$

The discrete WT splits a signal into approximations and details. The approximations are the high-scale, low-frequency components, and the details are the low-scale, high-frequency ones. The approximation itself is then split into a second-level approximation and detail, and the process is repeated till satisfactory results are obtained. Discrete WT decomposition tree is shown in Fig. 4. In some special applications, where the important information is located in higher frequencies, the decomposition process of only the approximation components at each level is not sufficient. Hence, in order to improve the time-frequency analysis, further decomposition of detail component to its own detail and of approximation components is necessary. This is called wavelet packet transform (WPT) which offers the richest analysis (Ref 29). Figure 5 shows the WPT tree for a signal s.

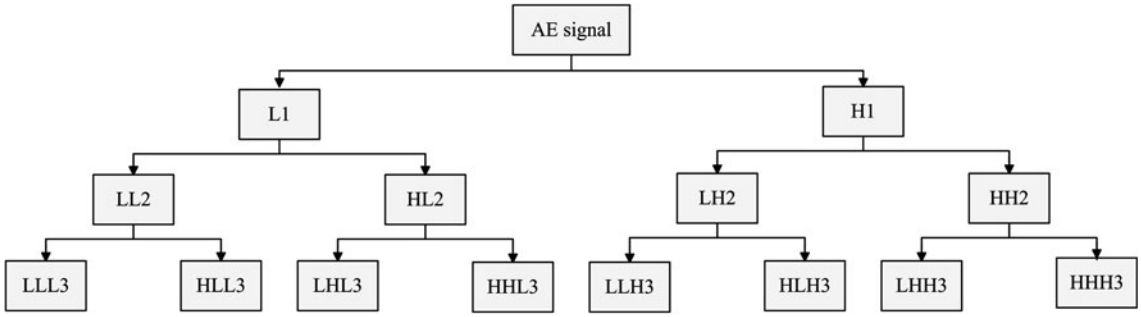

Fig 5 Wavelet packet transform tree

A wavelet packet $\psi^i_{j,k}$ can be defined using Eq 12:

$$\psi^i_{j,k} = 2^{-j/2}\psi^i(2^{-j}t - k), \quad i = 1, 2, \ldots, j^n \qquad \text{(Eq 12)}$$

where *i, j*, and *k* are the modulation, scale, and translation parameters, respectively, and *n* denotes the level of decomposition. The wavelet function ψ^i is obtained from the following recursive relationships:

$$\psi^{2i}(t) = \frac{1}{\sqrt{2}}\sum_{k=-\infty}^{+\infty} h(k)\psi^i\left(\frac{t}{2} - k\right) \qquad \text{(Eq 13)}$$

$$\psi^{2i+1}(t) = \frac{1}{\sqrt{2}}\sum_{k=-\infty}^{+\infty} g(k)\psi^i\left(\frac{t}{2} - k\right) \qquad \text{(Eq 14)}$$

The first two wavelet packet functions are the scaling and the mother wavelet functions:

$$\psi^0(t) = \phi(t) \qquad \text{(Eq 15)}$$

$$\psi^1(t) = \psi(t) \qquad \text{(Eq 16)}$$

The discrete filters $h(k)$ and $g(k)$ are quadrature mirror filters associated with the scaling function and the mother wavelet function.

The wavelet packet coefficients $c^i_{j,k}$ can be calculated from Eq 17:

$$c^i_{j,k} = \int_{-\infty}^{+\infty} f(t)\psi^i_{j,k}(t)\,dt \qquad \text{(Eq 17)}$$

The wavelet packet component $f^i_j(t)$ is obtained by Eq 18:

$$f^i_j(t) = \sum_{k=-\infty}^{+\infty} c^i_{j,k}\psi^i_{j,k}(t)\,\Delta t \qquad \text{(Eq 18)}$$

After performing the *j*th level of decomposition, the original signal is represented as Eq 19:

$$f(t) = \sum_{i=1}^{2^j} f^i_j(t) \qquad \text{(Eq 19)}$$

In this article, the energy criterion was employed to find the dominant components that were related to different damage modes.

If $f^j_1, \ldots, f^j_i$ denote the components of *j*th level of the decomposed signal, the component energy at level *j* can be calculated from Eq 20:

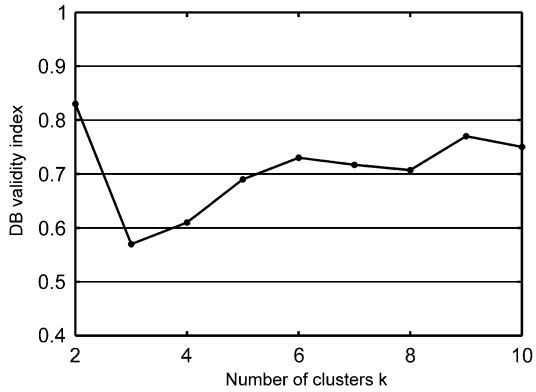

Fig. 6 DB index vs. the number of clusters (specimen S1)

$$E^i_j(t) = \sum_{\tau=t_0}^{t} (f^i_j(\tau))^2 \qquad \text{(Eq 20)}$$

Then the total energy of signal is defined by Eq 21:

$$E_{\text{Total}}(t) = \sum_j E^i_j(t) \qquad \text{(Eq 21)}$$

In order to find energy distribution displayed at different components, the ratio of energies at different levels to the total energy must be calculated. Equation 22 determines a relative energy distribution at each level:

$$p(t) = \frac{E^i_j(t)}{E_{\text{Total}}(t)}, \quad i = 1, \ldots, 2^j \qquad \text{(Eq 22)}$$

4. Results

During the three-point bending test of the specimens, S1 and S2, about 6000 and 10000 AE signals were detected, respectively. Six important AE features peak amplitude, rise time, count, energy, duration, and average frequency were extracted using the threshold value of 40 dB. In order to reduce the dimensionality of rather large dataset and better visualization of the data in a two-dimensional subspace, PCA was utilized. Since the variables (features) were not in same units, they were first standardized by their standard deviation. In this study, two first PCs were kept for clustering analysis. The cumulative sum of the variances of the two first PCs was about 86% of the total

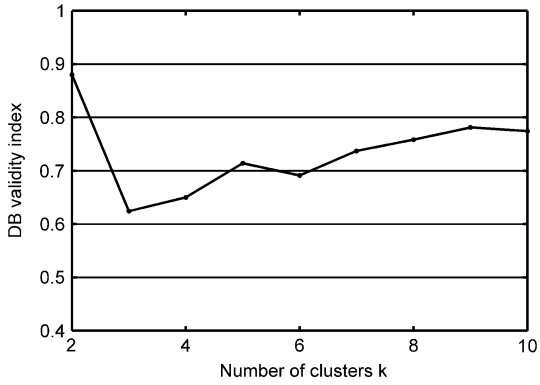

Fig. 7 DB index vs. the number of clusters (specimen S2)

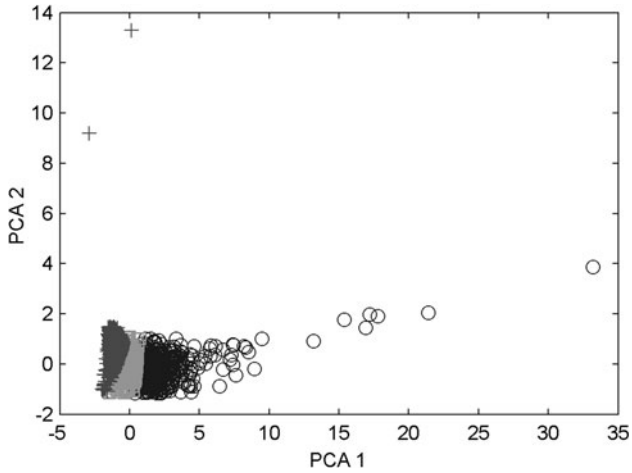

Fig. 8 PCA visualization of KGA clustering for specimen S1

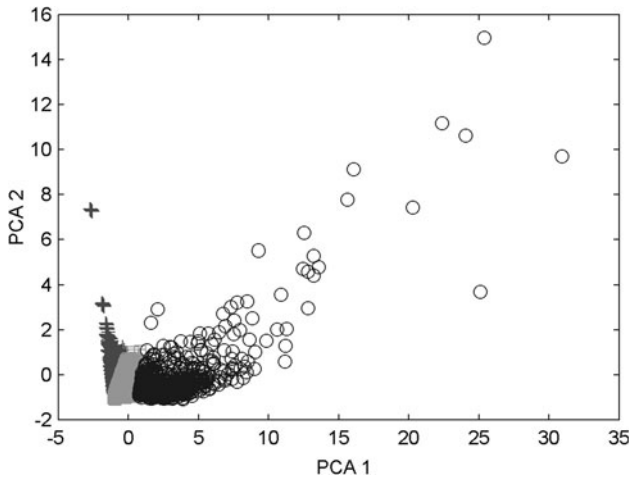

Fig. 9 PCA visualization of KGA clustering for specimen S2

variance of the input data for specimen S1, and 89% for specimen S2. After dimensional reduction, the AE signals were clustered using KGA. The optimum number of clusters was determined using Davis-Bouldin validity (DB) index. For this purpose, the KGA was executed with values of k from 2 to 10 and the DB index was calculated for each run. Figures 6 and 7 show average DB index versus the number of clusters (k).

Table 2 Distribution of AE signals in three clusters

Specimen	First cluster, %	Second cluster, %	Third cluster, %
S1	64	30	6
S2	16	27	57

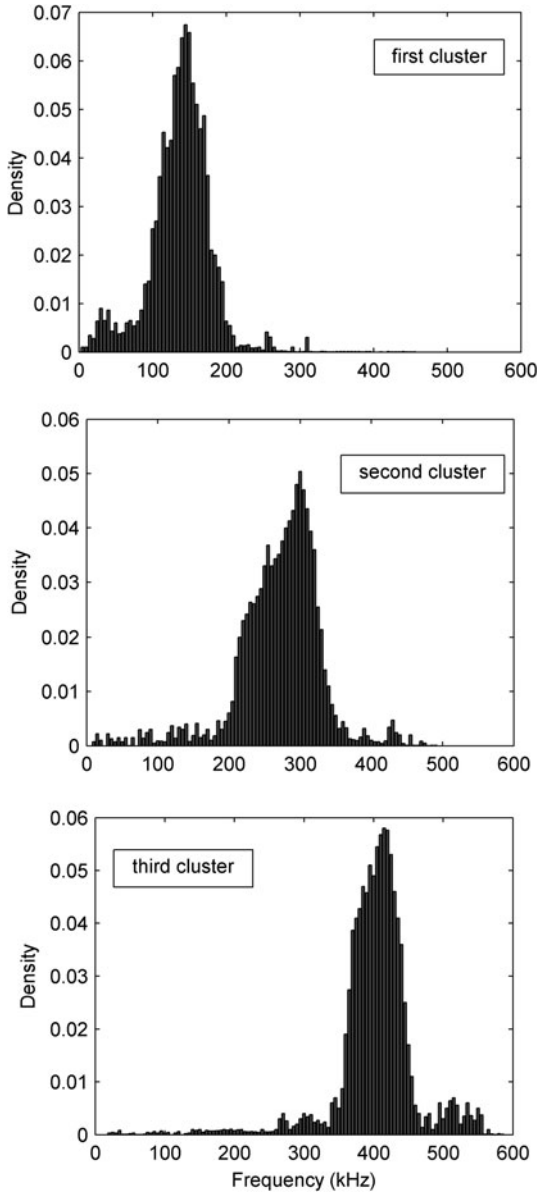

Fig. 10 Frequency distribution chart for specimen S1

The obtained results indicate that the optimum number of clusters which minimizes the DB index is three. PCA visualizations of KGA clustering are shown in Fig. 8 and 9. The results show that AE signals are well separated along the first principal direction. The distribution of AE signals in different clusters is summarized in Table 2. For the specimen S1, the first and the second clusters contain 94% of total AE signals. For the specimen S2, the second and the third clusters are more populated. About 84% of total AE signals are distributed in these two clusters.

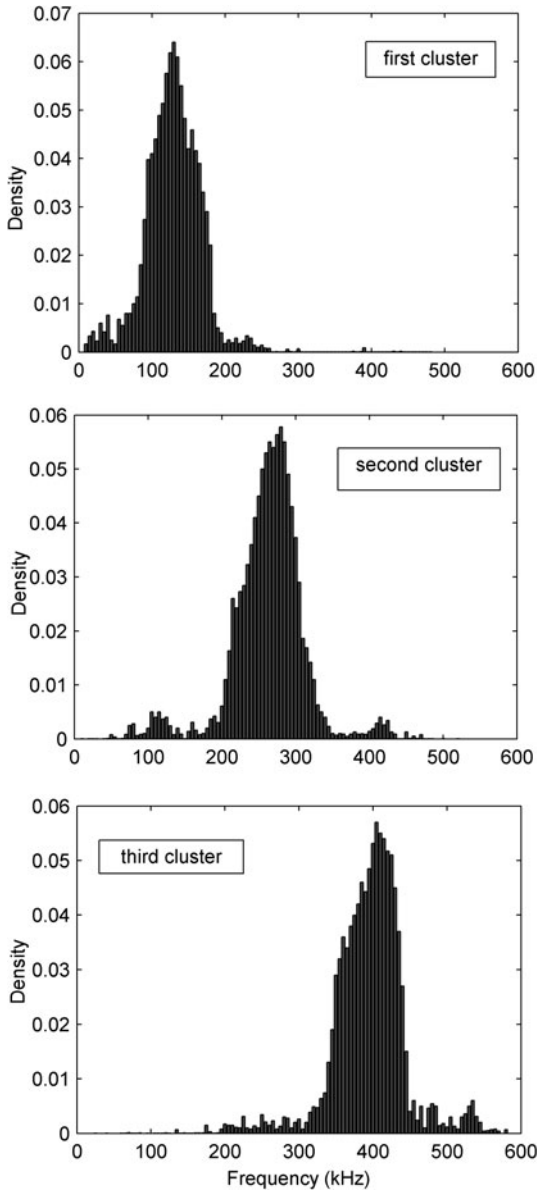

Fig. 11 Frequency distribution chart for specimen S2

Table 3 Frequency range of the obtained clusters

	Frequency range, kHz		
Specimen	**First class**	**Second class**	**Third class**
S1	90-195	210-335	360-450
S2	85-180	205-325	345-445

Since the datasets were labeled, mean AE parameters could be calculated for each cluster. Among different AE parameters, frequency was best distinguished. Hence, frequency was used as an efficient AE descriptor for damage characterization. The frequency contents of AE signals belonging to different clusters were obtained, and the frequency distribution charts were illustrated. Figures 10 and 11 show frequency distribution charts for the specimens, S1 and S2, respectively. The results

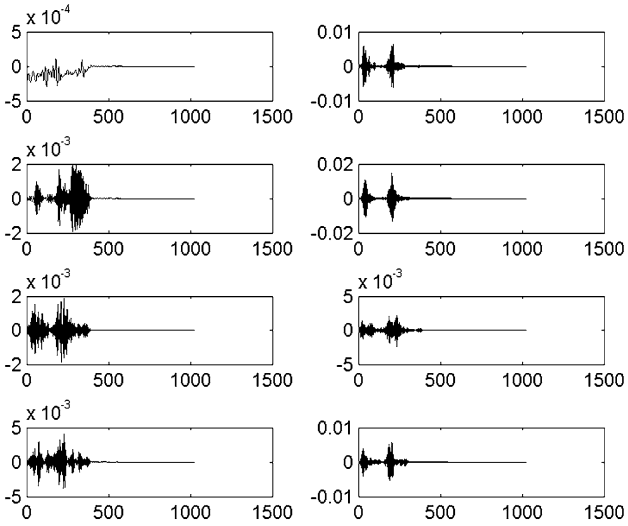

Fig. 12 Three-level wavelet packet decomposition of an AE signal for specimen S1 (amplitude in [mV] vs. samples)

highlight three separate frequency ranges for both specimens. Dominant frequency ranges of the obtained clusters are summarized in Table 3. It should be mentioned that, as shown in Fig. 10 and 11, there are some frequencies with low densities in each cluster that should be related to some other phenomena. Identification of these phenomena was not investigated in this study because they involve very small portions of AE events. The frequency ranges obtained by KGA were then compared with WPT results. For this purpose, AE signals were decomposed into three wavelet components using debauchees D10. The debauchees family was used based on the similarities between the AE signals and the wavelet family. Meanwhile, using trial and error method, db 10 was found the most appropriate among debauchees families, which could best match the AE signals. The entropy criterion was applied to define if further decomposition was necessary. Figure 12 shows the three-level WPT decomposition of an AE signal for the specimen S1. Each component represents a specific frequency range which can be obtained using FFT method (Fig. 13). With the aim of discriminating damage mechanisms, energy criterion was applied. The energy percentage of each component of level three was compared with the total energy of the AE signals based on the Eq 20-22. Figures 14 and 15 show energy distribution of level three components for the specimens, S1 and S2, respectively. The greatest percentage of energy is concentrated in the components LHL3, LLH3, and LHH3. For the specimen S1, the most dominant components are LHL3 and LLH3, while for the specimen S2, the most significant ones are LLH3 and LHH3 from energy point of view. It is clear that the energy distribution pattern at the same component is different for different specimens. This difference is because of different major damage mechanisms for each specimen.

Table 4 summarizes the frequency range of dominant components. These results are in good consistency with KGA outputs (see Table 3).

According to the previous studies conducted in this field (Ref 17, 20, 30), there are three prevalent damage mechanisms for fiber-reinforced composite materials: matrix cracking, fiber-matrix debonding and fiber breakage. SEM observation taken in the vicinity of starter crack illustrates

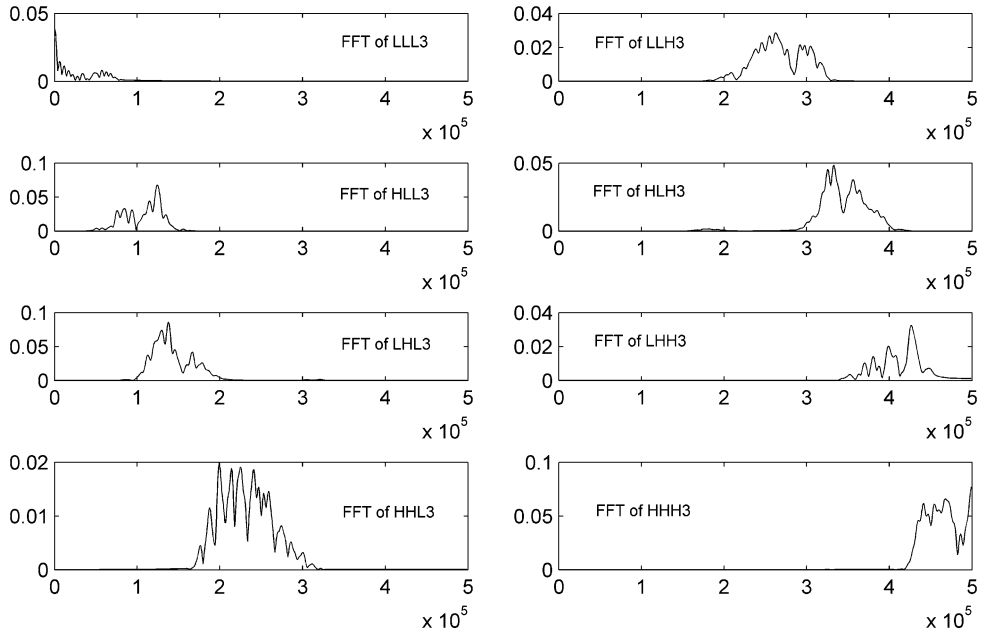

Fig. 13 Level 3 FFT of the decomposed components (FFT amplitude [mV2/Hz] vs. frequency [Hz])

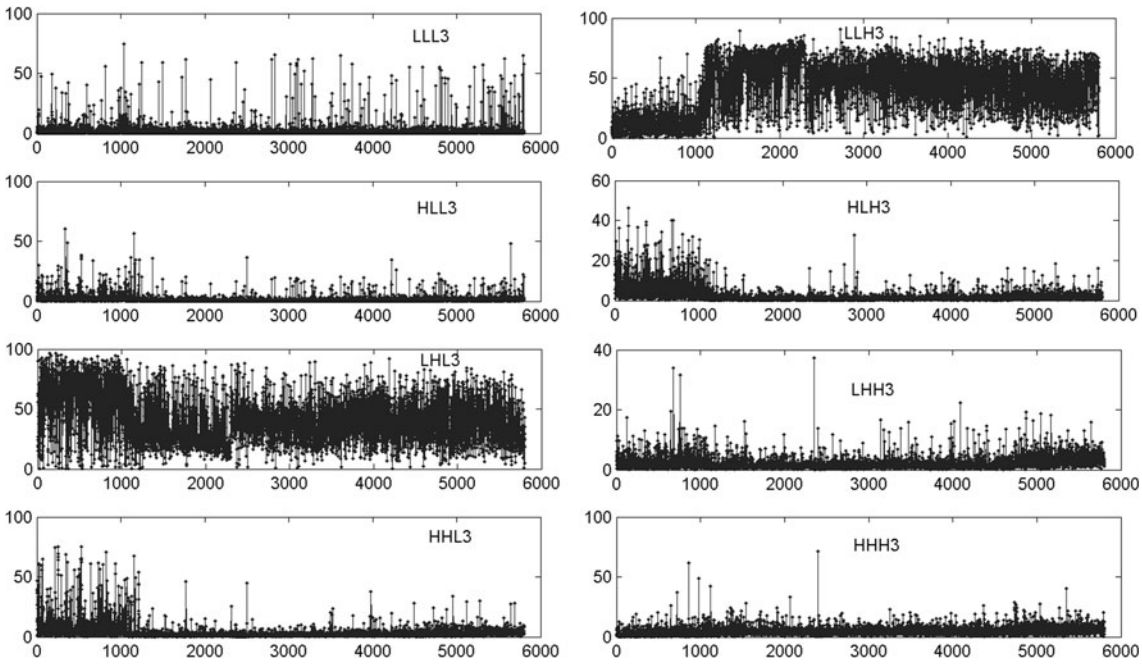

Fig. 14 Energy percentage of each component of Level 3 for S1 (energy [%] vs. samples)

these failure mechanisms. As shown in Fig. 16, for the specimen, S1, matrix cracking and fiber-matrix debonding, are the most dominant failure modes. However, a little fiber breakage was also observed. For the specimen, S2, fiber breakage and debonding are the most significant failure modes (Fig. 17). Considerable fiber breakage in the specimen, S2, can be related to fiber-bridging phenomenon in unidirectional composites.

In order to correlate the AE signals of each cluster to a distinct damage mechanism, the relationship between frequency contents and damage mechanisms was considered. The relationship between frequency ranges and damage mechanisms could be found based on the different visco-elastic relaxation processes near the damage sources (Ref 31, 32). Intrinsic frequencies f_i and elastic acoustic velocities of relaxation processes rely on the elastic moduli and density as shown in Eq 23 (Ref 32):

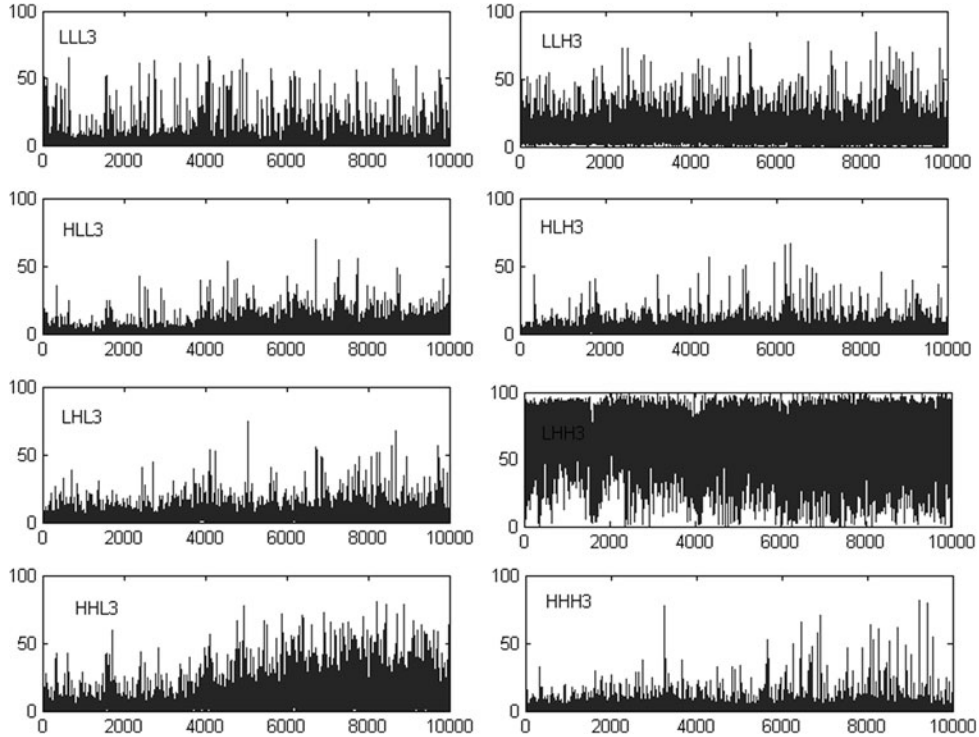

Fig. 15 Energy percentage of each component of Level 3 for S2 (energy [%] vs. samples)

Table 4 Frequency range of dominant components

Component	LHL3	LLH3	LHH3
Frequency range, kHz	100-190	200-320	355-450

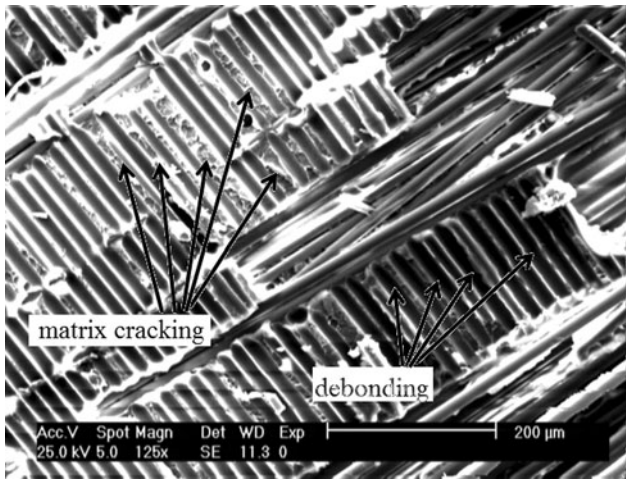

Fig. 16 SEM observation of dominant failure mechanisms (specimen S1)

$$f_i \sim \frac{1}{\tau_i} \sim c_i \sim \sqrt{\frac{E_i}{\rho_i}} \qquad \text{(Eq 23)}$$

where τ_i is the relaxation time, ρ_i is the density and E_i is the elastic modulus.

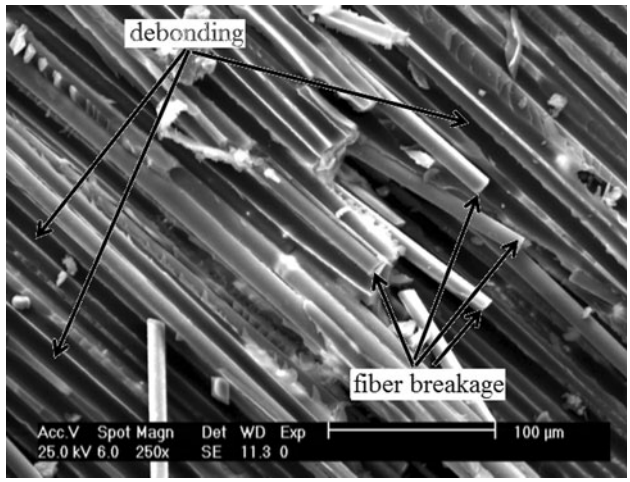

Fig. 17 SEM observation of dominant failure mechanisms (specimen S2)

According to the Eq 23, the lowest and the highest frequencies are related to matrix (epoxy) cracking and fiber (glass) breakage, respectively. The frequency contents of glass-epoxy debonding are between frequency contents of matrix cracking and fiber breakage.

Hence, it can be concluded that the AE signals of the first cluster are representatives of matrix cracking, while the AE signals of the second and the third clusters are associated with fiber-matrix debonding and fiber breakage, respectively.

As mentioned above, for the specimen, S1, matrix cracking and debonding are the most significant damage mechanisms. These two mechanisms contain 94% of total AE activities of specimen S1 (see Table 2). For the specimen, S2, debonding

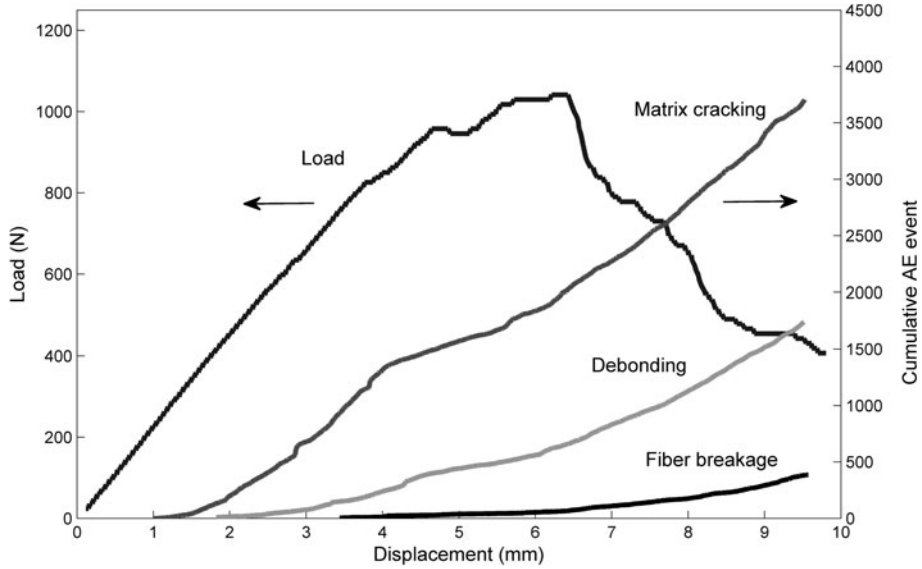

Fig. 18 Load-displacement data and sequence of damage mechanisms (specimen S1)

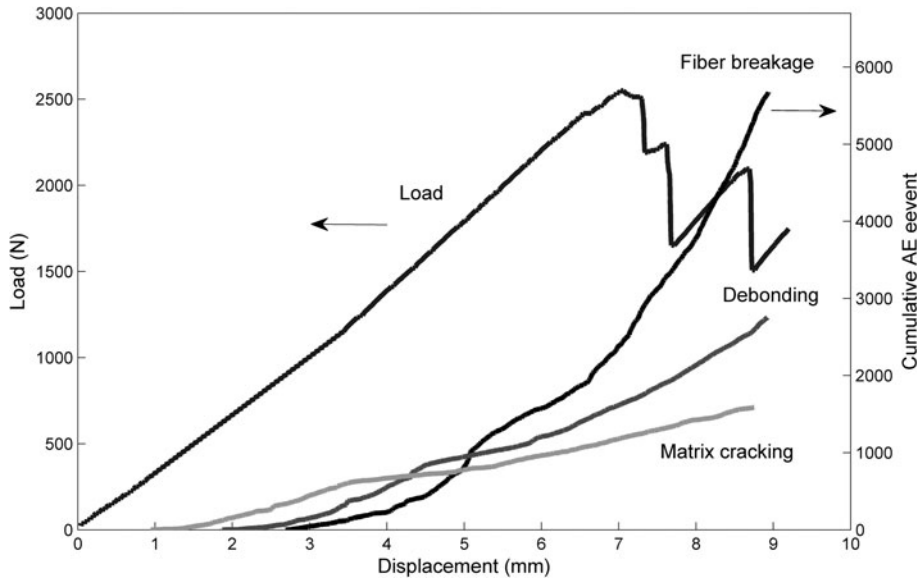

Fig. 19 Load-displacement data and sequence of damage mechanisms (specimen S2)

and fiber breakage are the most dominant failure mechanisms. About 84% of AE activities are associated with these two mechanisms.

Also the sequence of damage mechanisms is illustrated in Fig. 18 and 19. The figures show load-displacement data as well as the order of damage mechanisms. For both the specimens, matrix cracking is the earliest damage mode that appears from the beginning of the tests, while debonding and fiber breakage happen later. For the specimen, S2, fiber breakage grows faster than the two other damage mechanisms do and contains much more AE events, especially at the final stages of the experiments. For the specimen, S1, matrix cracking is the most predominant damage mode. However, debonding is also increasing till the end of the tests.

5. Conclusion

The aim of this study was to develop efficient methods to discriminate different damage mechanisms of glass/epoxy composites. For this purpose, integration of *k*-means algorithm and genetic algorithm was applied to cluster AE activities. Using Davis-Bouldin validity (DB) index, three clusters with separate frequency ranges were achieved. Each frequency range was related to a distinct damage mode. The outputs of KGA were then compared with WPT results. First, AE signals were decomposed into three levels, and then the energy distribution criterion was used to find the dominant components. Three components LHL3, LLH3 and LHH3 with frequency ranges at 100-190, 200-320, and 355-450 kHz, respectively, were the

most significant from the energy criterion point of view. The frequency ranges obtained by WPT were in good consistency with KGA outputs. Also, in this study, SEM observation was used for validating the results. SEM observation revealed that the damage mechanisms of matrix cracking, debonding, and fiber breakage were the sources of AE signals. Considering the relationship between frequency ranges and damage mechanisms, the AE signals of each cluster were assigned to a distinct damage mechanism. It was concluded that the AE signals of the first cluster were related to matrix cracking, and the those of the second and the third clusters were representative of fiber-matrix debonding and fiber breakage, respectively. According to the distribution of AE signals in different clusters, matrix cracking and debonding were the most significant damage mechanisms for the specimen S1, while debonding and fiber breakage were the most dominant failure mechanisms for the specimen S2.

Acknowledgment

The authors wish to thank the Department of Mechanical Engineering at Amirkabir University of Technology, for providing the facilities for this study.

References

1. W. Chen, Some Experimental Investigations in the Drilling of Carbon Fiber-Reinforced Plastic (CFRP) Composite Laminates, *Int. J. Mach. Tools Manuf.*, 1997, **37**(8), p 1097–1108
2. S.R. Ravishankar and C.R.L. Murthy, Application of Acoustic Emission in Drilling of Composite Laminates, *NDT&E Int.*, 2000, **33**(6), p 429–435
3. K.M. Ronnie, *Handbook of Nondestructive Testing*, Vol 5, *Acoustic Emission*, 2nd ed., American Society for Nondestructive Testing, 1987
4. T.M. Ely and E.K. Hill, Longitudinal Splitting and Fibre Breakage Characterization in Graphite/Epoxy Using Acoustic Emission Data, *Mater. Eval.*, 1995, **53**(2), p 288–294
5. T. Uenoya, Acoustic Emission Analysis on Interfacial Fracture of Laminated Fabric Polymer Matrix Composite, *J. Acoust. Emiss.*, 1995, **13**(3–4), p 95–102
6. S. Barré and M.L. Benzeggagh, On the Use of Acoustic Emission to Investigate Damage Mechanisms in Glass-Fibre-Reinforced Poly-Propylene, *Compos. Sci. Technol.*, 1994, **52**(3), p 369–376
7. N. Ativitavas, T. Fowler, and T. Pothisiri, Acoustic Emission Characteristics of Pultruded Fiber Reinforced Plastics Under Uniaxial Tensile Stress, *Proceedings of European WG on AE* (Berlin), 2004, p 447–454
8. G.N. Morscher, J. Martinez-Fernandez, and M.J. Purdy, Determination of Interfacial Properties Using a Single-Fiber Microcomposite Test, *J. Am. Ceram. Soc.*, 1996, **79**(4), p 1083–1091
9. K. Yamaguchi, H. Oyaizu, J. Johkaji, and Y. Kobayashi, Acoustic Emission Technology Using Multi-Parameter Analysis of Waveform and Application to GFRP Tensile Tests, *Acoustic Emission, Current Practice and Future Directions,* ASTM STP 1077, Philadelphia, PA, 1991, p 123–143
10. Y.Z. Pappas, Y.P. Markopoulos, and V. Kostopoulos, Failure Mechanisms Analysis of 2D Carbon/Carbon Using Acoustic Emission Monitoring, *NDT&E Int.*, 1998, **31**(3), p 157–163
11. V. Kostopoulos, T.H. Loutas, A. Kontsos, G. Sotiriadis, and Y.Z. Pappas, On the Identification of the Failure Mechanisms in Oxide/Oxide Composites Using Acoustic Emission, *NDT&E Int.*, 2003, **36**(8), p 571–580
12. K. Kenji and K. Ono, Pattern Recognition of Acoustic Emission Signals from Carbon Fiber/Epoxy Composites, *7th International Acoustic Emission Symposium* (Zao, Japan), 1987
13. M. Moevus, N. Godin, M. R'Mili, D. Rouby, P. Reynaud, G. Fantozzi, and G. Farizy, Analysis of Damage Mechanisms and Associated Acoustic Emission in Two SiCf/[Si-B-C] Composites Exhibiting Different Tensile Behaviours. Part II. Unsupervised Acoustic Emission Data Clustering, *Compos. Sci. Technol.*, 2008, **68**(6), p 1258–1265
14. T.P. Philippidis, V.N. Nikolaidis, and A.A. Anastassopoulos, Damage Characterization of Carbon/Carbon Laminates Using Neural Networks Techniques on AE Signals, *NDT&E Int.*, 1998, **31**(5), p 329–340
15. T. Yan, K. Holford, D. Carter, and J. Brandon, Classification of Acoustic Emission Signatures Using a Self-Organization Neural Network, *J. Acoust. Emiss.*, 1999, **17**(1/2), p 49–59
16. R. de Oliveira and A.T. Marques, Health Monitoring of FRP Using Acoustic Emission and Artificial Neural Networks, *Comput. Struct.*, 2008, **86**(3–5), p 367–373
17. N. Godin, S. Huguet, and R. Gaeertner, Integration of the Kohonen's Self-Organizing Map and *k*-Means Algorithm for the Segmentation of the AE Data Collected During Tensile Tests on Cross-Ply Composites, *NDT&E Int.*, 2005, **38**(4), p 299–309
18. S. Haykin, *Neural Networks—A Comprehensive Foundation*, 2nd ed., Macmillan College, New York, 1994
19. Q.-Q. Ni and M. Iwamoto, Wavelet Transform of Acoustic Emission Signals in Failure of Model Composites, *Eng. Fract. Mech.*, 2002, **69**(6), p 717–728
20. A. Marec, J.H. Thomas, and R. El Guerjouma, Damage Characterization of Polymer-Based Composite Materials: Multivariable Analysis and Wavelet Transform for Clustering Acoustic Emission Data, *Mech. Syst. Signal Process.*, 2008, **22**(6), p 1441–1464
21. I.T. Jolliffe, Principal Component Analysis, 2nd ed., Springer Series in Statistics, 2002
22. A. Likas, N. Vlassis, and J. Verbeek, The Global *k*-Means Clustering Algorithm, *Pattern Recognit.*, 2003, **366**(2), p 451–461
23. D.L. Davies and D.W. Bouldin, A Cluster Separation Measure, *IEEE Trans. Pattern Anal. Mach. Intell.*, 1979, **1**(4), p 224–227
24. C.A. Murthy and N. Chowdhury, In Search of Optimal Clustering Using Genetic Algorithms, *Pattern Recognit. Lett.*, 1996, **17**(8), p 825–832
25. S. Bandyopadhyay and U. Maulik, An Evolutionary Technique Based on *k*-Means Algorithm for Optimal Clustering in R^N, *Inf. Sci.*, 2002, **146**(1–4), p 221–237
26. A. Grossmann and J. Morlet, Decomposition of Hardy Functions into Square Integrable Wavelets of Compact Shape, *SIAM J. Math. Anal.*, 1984, **15**(4), p 723–736
27. G. Qi, Wavelet-Based AE Characterization of Composite Materials, *NDT&E Int.*, 2000, **33**(3), p 133–144
28. T.H. Loutas, V. Kostopoulos, C. Ramirez-Jimenez, and M. Pharaoh, Damage Evolution in Center-Holed Glass/Polyester Composites Under Quasi-Static Loading Using Time/Frequency Analysis of Acoustic Emission Monitored Waveforms, *Compos. Sci. Technol.*, 2006, **66**(10), p 1366–1375
29. R.R. Coifman, Y. Meyer, S.R. Quake, and M.V. Wickerhauser, Signal Processing and Compression with Wavelet Packets, *Progress in Wavelet Analysis and Applications*, Y. Meyer and S. Roques, Ed., Editions Frontières, 1993, p 77–93
30. A.R. Oskouei, M. Ahmadi, and M. Hajikhani, Wavelet-Based Acoustic Emission Characterization of Damage Mechanisms in Composite Materials Under Mode I, Delamination at Different Interfaces, *eXPRESS Polym. Lett.*, 2009, **3**(12), p 804–813
31. M. Giordano, L. Condelli, and L. Nicolais, Acoustic Emission Wave Propagation in a Viscoelastic Plate, *Compos. Sci. Technol.*, 1999, **59**(11), p 1735–1743
32. J. Bohse, Acoustic Emission Characteristics of Micro-Failure Processes in Polymer Blends and Composites, *Compos. Sci. Technol.*, 2000, **60**(8), p 1213–1226